Adsorption 4, 207–224 (1998)

Capillary Condensation and Melting/Freezing Transitions for Methane in Slit Coal Pores

ALEKSEY VISHNYAKOV, ELENA M. PIOTROVSKAYA AND ELENA N. BRODSKAYA

Department of Chemistry, St. Petersburg State University, Universitetsky pr. 2, 198904, St. Petersburg, Russia

Abstract. Grand canonical Monte Carlo method has been applied to study the adsorption behavior of methane in slit coal micropores for pore widths from 1.5 to 4.5 nm at temperatures 111–300 K. The adsorbent surface is considered to be inhomogeneous with C, N, S, O and H atoms, as well as vacancies, taken into account. The effect of surface microstructure on mechanism of the pore filling and saturation pressure is found to be more pronounced at relatively low and moderate strength of the adsorption field. It is also shown that irregular impurities and defects at the adsorbent surface contribute to the lowering of the freezing temperature and can change qualitively its dependence on the pore width.

Keywords: carbon adsorbents, pore condensation, computer simulation

1. Introduction

Scientific interest in phase transitions in micropores springs from wide application of microporous solids for mixture separation, waste cleanup, heterogeneous catalysis etc. Becides, many rock and soil formations as well as mining coals are porous. Experimental (e.g., Thommes et al., 1994; Morishige et al., 1997), theoretical (see, e.g., Fundamentals of Adsorption Conference, 1993), and computer simulation studies over the last decade contributed substantially to the understanding of the nature of layering transitions and capillary condensation in pores. Conditions of the liquid-vapor equilibrium for simple fluids in micropores of various width, shape and adsorption potential were obtained by Peterson and Gubbins (1987), Jiang et al. (1993), Piotrovskaya and Brodskaya (1995), etc. Less investigated are melting and freezing transitions in micropores. Several experimental studies of freezing and melting on well-characterized porous materials have been reported. Both decrease (Unruh et al., 1993; Molz et al., 1993; Warnock et al., 1986) and increase (Klein and Kumacheva, 1995) in melting temperature on confinement were observed for different adsorbed fluids and pore materials. Melting temperatures were higher than those for freezing, showing hysteresis effects. The influence of the pore shape and material on freezing temperatures remain unclear.

In computer simulation freezing transitions were observed in cylindrical (Peterson et al., 1990) and slit (Jiang et al., 1993) pores. A systematic grand canonical Monte Carlo (GCMC) study of methane melting and freezing in slit pores was recently reported by Miyahara and Gubbins (1997), with the main attention paid to the dependence of the freezing temperature on the pore width and the strength of the adsorption field. For graphite pores the freezing temperature was higher than that of the bulk material and increased with the decrease of the pore width; pores with hard walls showed a decrease in the freezing temperature on confinement; for pores with the walls having the adsorption field corresponding to that of solid methane no significant shift in the freezing temperatures relative to the bulk methane was observed. So, the authors concluded that freezing and melting temperatures depend strongly on the adsorption field of the pore material. Both structured and structureless graphite was examined; the influence of the graphite structure on freezing and melting temperatures was found to be negligible.

However, most theoretical studies did not go beyond simple capillary models with perfect symmetry.

Information concerning the influence of the surface heterogeneity on the nature and conditions of phase transitions in pores is rather poor. Gac et al. (1993) studied capillary condensation of a lattice gas with a simple cubic structure in pores with chemical inhomogeneity produced by a periodic wall potential using GCMC. Similar systems were considered by Röcken and Tarazona (1996) using a nonlocal density functional theory. The authors of both papers observed a new two-stage mechanism of capillary condensation. Muller and Gubbins (1996) performed Gibbs ensemble Monte Carlo simulation of water adsorption in slit pores with uniform graphite walls, on which square–well active sites were placed. The condensation pressure was found to be shifted to considerably lower pressures by the presence of the active sites. At higher site concentrations capillary condensation was no longer observed: water molecules adsorbed on the active sites and formed clusters around these sites. Capillary condensation of Lennard-Jones argon in cylindrical pores with hard geometrically heterogeneous walls was studied by Steele and Bojan (1996). In spite of significant changes in the density profile, caused by pore wall heterogeneity, almost no shift in the condensation point was observed.

The present work deals with the adsorption of Lennard-Jones methane in slit micropores, formed by mining coals. Mining coals were considered to be polycrystalline materials with graphite-type structure, including some impurities (mostly O, S, N and H atoms in various functional groups) and vacancies. These defects make the adsorbent surface geometrically and energetically heterogeneous; dependent on the atomic structure of the surface, some places become more active adsorbing sites. Densities and composition (including the distribution of atoms by functional groups) has been widely measured for different mining coals. Nevertheless, the information on the distribution of surface defects in crystalline lattice for coals is quite poor (see, e.g., Eremin et al., 1980). This leaves significant freedom for modeling coal surface. In the present work we consider sample structures with various pore wall heterogeneity in order to estimate its influence on the molecular structure and parameters of phase transitions of the adsorbate. The sample structures considered were designed using experimental data on density, structure and composition of mining coals of Eremin et al. (1980). Another goal of this work is to study the dependence of various properties of the adsorbate on the pore width.

2. Models and Simulation Technique

2.1. Potential Models

The molecules of methane were treated as one-site sphericals; their interactions with each other and the elements of the coal surface were represented by the truncated Lennard-Jones (LJ) potential

$$\Phi_{\alpha\beta}(r) = 4\epsilon_{\alpha\beta}\left(\left(\frac{\sigma_{\alpha\beta}}{r}\right)^{12} - \left(\frac{\sigma_{\alpha\beta}}{r}\right)^{6}\right), \qquad (1)$$

where $\sigma_{\alpha\beta}$ and $\epsilon_{\alpha\beta}$ are, respectively, the LJ size and energy parameters for the interaction of sites α with β. All functional groups and LJ parameters used are listed in Table 1. Parameters for interaction of methane molecule with graphitic carbon atom, aromatic CH group and sulfur were optimized taking in account thermodynamic properties of adsorbed monolayers (see Bojan et al., 1992). LJ parameters for the other groups were developed to fit the experimental data on structure and thermodynamic properties of bulk hydrocarbons, alchohols, organic acids and amines (Weiner et al., 1984; Jorgensen et al., 1984; Jorgensen, 1986; Jorgensen and Gao, 1986); we, however, believe, that they can give a fair description of interactions between methane and the elements of the solid. The cut-off distance was 3.2σ (here and further on σ and ϵ denote the LJ parameters for fluid-fluid interaction). The

Table 1. Lennard-Jones parameters for fluid-fluid and fluid-solid interactions. σ and ϵ are the parameters for a pair of methane molecules.

	α	$\sigma_{\alpha\text{-}CH_4}$ (nm)	$\epsilon_{\alpha\text{-}CH_4}$ (J/mol)	$\sigma_{\alpha\text{-}CH_4}/\sigma$	$\epsilon_{\alpha\text{-}CH_4}/\epsilon$
1	CH_4	0.373	1229.8	1	1
2	CH(arom.)	0.356	786.1	0.931	0.639
3	C(arom.)	0.3600	548.5	0.942	0.420
4	S(arom.)	0.375	1662	0.980	1.351
5	OH(CH)	0.345	937.1	0.903	0.760
6	NH_2	0.353	937.0	0.920	0.760
7	CH_3	0.386	780.7	0.994	0.706
8	O(CO)	0.3390	1041.5	0.880	0.846
9	C(CO)	0.3785	735.6	0.990	0.598
10	CH	0.3835	642.1	1.003	0.552
11	CH(=)	0.3810	769.9	0.997	0.626

slit pores we deal with here are formed by two planar surfaces of solid, parallel to the xy plane. Adsorbent surface was composed of periodically repeated identical fragments according to periodic boundary conditions implied in x and y directions. Fragments of some of the coal structures considered are shown in Fig. 1. The elements of the solid were immobile. Long ranged fluid-solid interactions were taken into account as if the surface was uniform; for fluid-fluid interactions no long-range correction was included. Only the first lattice layer of the adsorbent was considered to be structured. The others were producing 10-4-3 potential (Steele, 1974):

$$\Phi_{s\alpha}(z) = 2\pi\Delta \sum_{\alpha} \rho_\alpha \epsilon_{f\beta} \sigma_{f\alpha}^2 \left(\frac{2}{5} \left(\frac{\sigma_{f\alpha}}{z} \right)^{10} - \left(\frac{\sigma_{f\alpha}}{z} \right)^4 - \frac{\sigma_{f\beta}^4}{3\Delta(z + 0.61\Delta)^3} \right), \quad (2)$$

where ρ_α is the surface density of sites α, z is the distance between a fluid molecule and the solid surface, Δ is the separation between neighbouring lattice layers. For graphite-type structure $\Delta = 0.335$ nm, the length of the C─C bond is 0.142 nm.

2.2. *Adsorbents*

We consider several samples of the coal structure. These samples represent different stages of coal metamorphism. They differ in density, composition and the nature of defects they contain. First, we consider both structured and structureless graphite. Since no substantial difference in fluid behavior between these two systems was found, both of these pores will be called as system I. Secondly, we consider the structure shown in Fig. 1(a) (this pore is referred to as system II). This is a typical mining anthracite with a pronounced graphite-type structure, composed of aromatic carbon atoms (86% of mass), some impurities (14%), and vacancies. The structure shown in Fig. 1(b) (system III), includes a larger amount of impurities (25% of mass) and vacancies, which form holes up to 0.52σ in diameter. Systems II and III have relatively uniform surfaces and rather strong adsorption field, close to that of graphite (I). In these pores fluid molecules cannot approach the second lattice plane. It becomes possible in system IV, which contains about 40% of impurities. Vacancies form holes up to 0.75σ in diameter. It makes these holes preferential adsorption sites. As

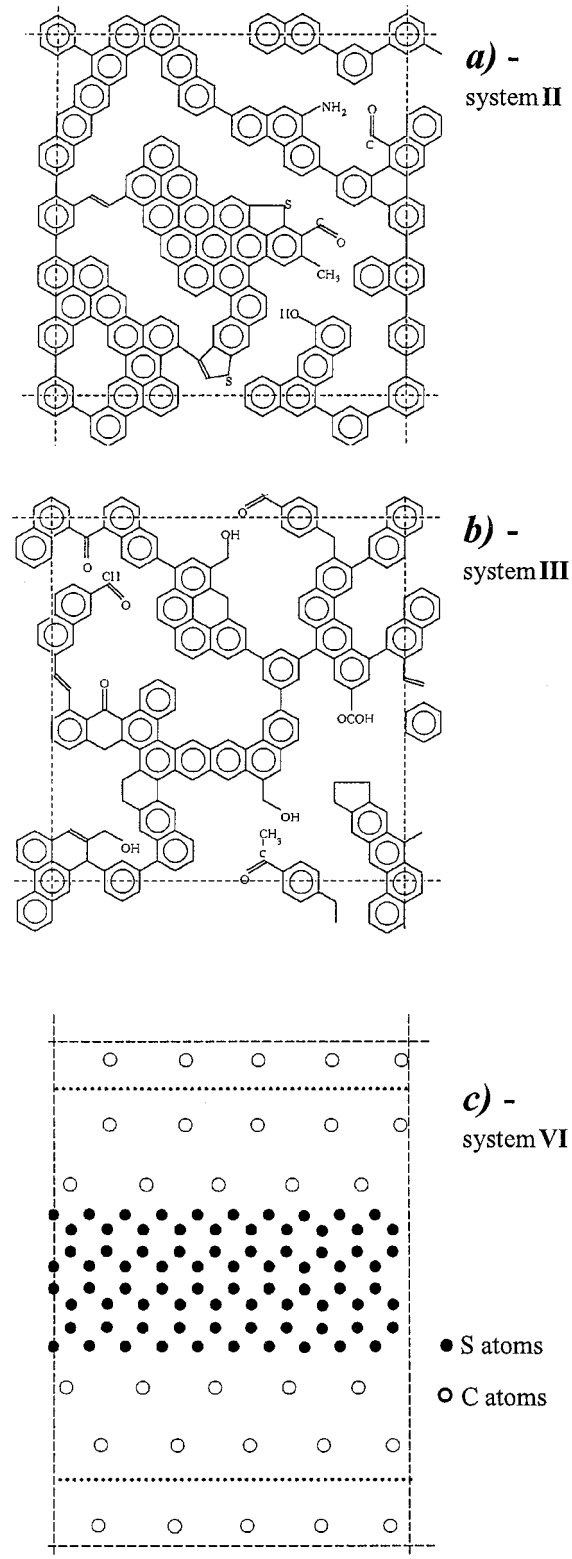

Figure 1. Samples of coal surface structure: (a) system II, (b) system III, and (c) system VI.

a reference system for system IV we also consider a pore with the average adsorption characteristics equal to those of system IV but with uniform 10-4-3 walls (system V).

Finally, we consider an adsorbent, where strongly attractive sites form a strip on the surface—system VI (Fig. 1(c)). The strongly adsorbing strip was composed of sulfur atoms (No. 4 from Table 1), the weakly adsorbing part of the surface—of aromatic carbon atoms (No. 3 from Table 1). The energy of adsorption of a methane molecule at the surface composed of sulfur atoms only would be $U_{\text{strong}} = -26.3\epsilon$. The energy of adsorption of a fluid molecule on this part U_{weak} varied from -1.0 to -5.0ϵ. As periodic boundary conditions were applied in x and y directions, the pore surface had a periodic structure; in order to make the behavior of the fluid in strongly adsorbing parts mutually independent, the size of the basic cell in y direction L_y was enlarged by factor 3 compared to systems II–IV. In order to study the influence of the ratio between the width of the strip L_s and pore width H on the mechanism of capillary condensation, we considered strips of several widths: $L_s = 2.4\sigma, 3.2\sigma$ and 4.8σ, which corresponded to 9, 12 and 18 rows of sulfur sites, respectively.

To demonstrate the inhomogeneity of the surface, the minimum energy of fluid-solid interaction (further on called a local energy of adsorption $U_{\text{ads}}(x, y)$) is shown in Fig. 2 as a function of the location of a fluid molecule over the surface. Geometrical inhomogeneity can be characterized by the distance $z_{\text{ads}}(x, y)$ between the fluid molecule and the adsorbent surface, where $U_{\text{ads}}(x, y)$ is achieved. Average characteristics of all these adsorbents are given in Table 2. Systems IP and IIP in Table 2 correspond to the systems I and II from the earlier work of Piotrovskaya and Brodskaya (1995), where 9-3 potential was used to present fluid-solid interactions.

2.3. *Simulation Details*

Grand canonical Monte Carlo method was used. The pore width H, which is the distance between the planes of the nuclei of the first lattice layers of the adsorbent, varied from 4.0 to 10.0σ. In simulations with systems II, III, IV the adsorbent surface area was $L_x \times L_y = 6.660\sigma \times 6.405\sigma$, for system VI—$6.660\sigma \times 19.25\sigma$, for systems I, V—$10.0\sigma \times 10.0\sigma$, according to the size of the coal surface fragment. The runs were usually 20,000–40,000 steps per molecule, up to 200,000 steps per molecule when necessary. In order to fix freezing/melting transitions in some systems, diffusion coefficients in the direction parallel to the walls were estimated using molecular dynamics (MD) simulations in canonical ensemble. The initial configurations for MD were obtained from GCMC, then equillibration and temperature scaling were carried out by MD over 5 ns, then statistics were collected over 2 ns. Time step was 10^{-5} ns. The diffusion coefficients were calculated using the time dependence of the mean-square displacements.

2.4. *Grand Potential Calculation*

To determine the location of the liquid-vapor phase coexistence at a given temperature T, we calculated the dependence of the grand potential Ω, on the chemical potential μ separately for the vapor and liquid phases (Peterson and Gubbins, 1987). The intersection of two branches of the isotherm for Ω corresponds to the point of phase equilibrium and gives the value of μ_{coex}. In

Table 2. Average characteristics of the adsorbents: average energy of adsorption of methane molecule $\bar{U}_{\text{ads}}$ and its mean square deviation $\triangle U_{\text{ads}}$, average distance from the wall where $\bar{U}_{\text{ads}}$ is achieved $\bar{z}_{\text{min}}$ and its mean square deviation $\triangle z_{\text{ads}}$.

System	Description	$\bar{U}_{\text{ads}}/\epsilon$	$\triangle U_{\text{ads}'}/\epsilon$	$\bar{z}_{\text{ads}'}/\sigma$	$\triangle z_{\text{ads}}/\sigma$
I	Crystalline garphite	−8.42	0.08	0.930	0.007
I	Graphite 10-4-3	−8.42	0	0.930	0
II	Anthracite, 86% aromatic carbon	−8.07	0.53	0.932	0.034
III	Anthracite, 75% aromatic carbon	−7.58	0.86	0.935	0.056
IV	Coal, 60% aromatic carbon	−4.25	1.17	0.930	0.141
V	Structureless coal, 10-4-3	−4.25	0	0.893	0
IP	Graphite 9-3	−7.82	0	0.603	0
IIP	Structureless coal, 9-3	−3.91	0	0.603	0

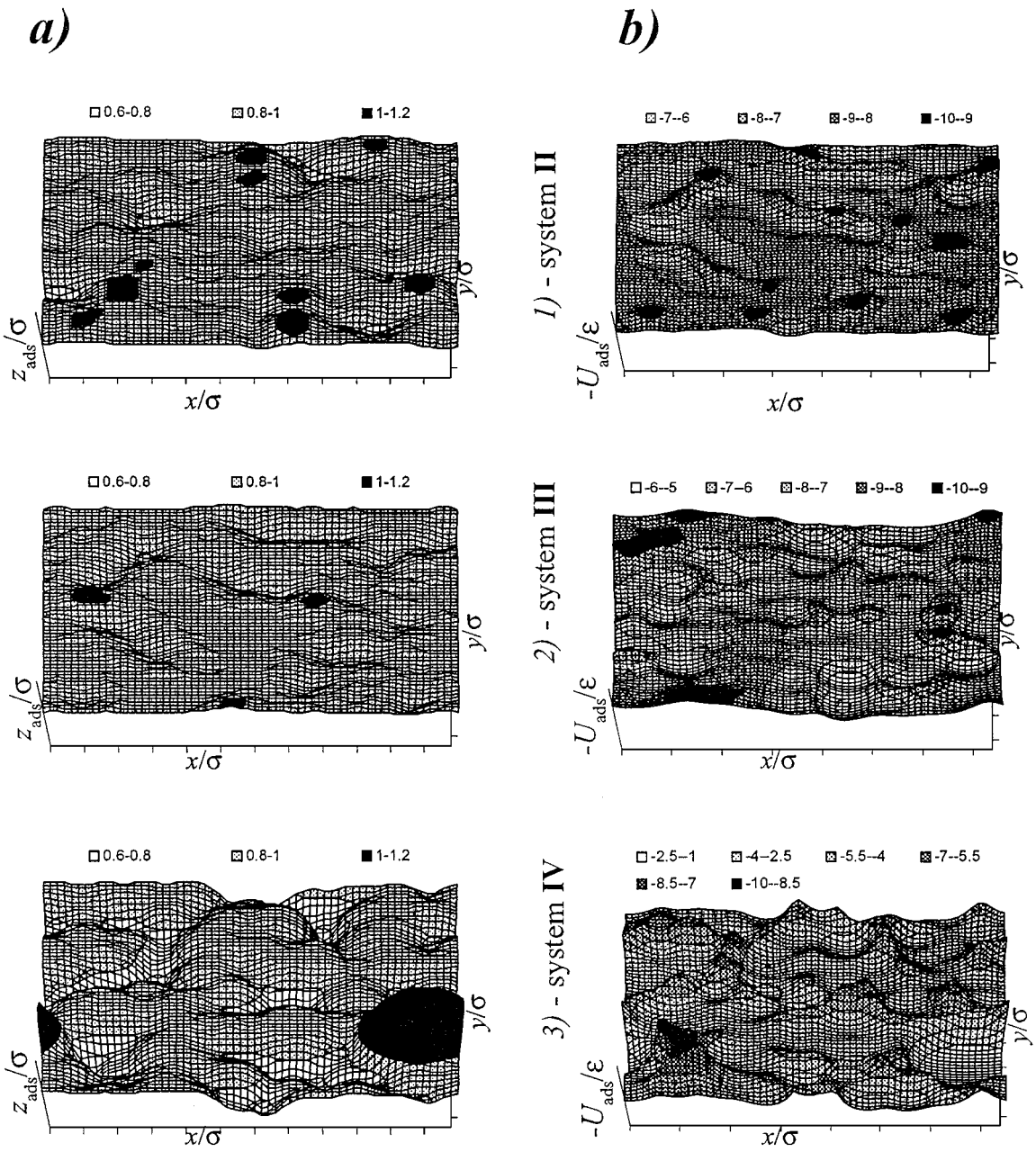

Figure 2. Map of the local energy of adsorption U_{ads} (a) and the distance from a fluid molecule to the coal surface z_{ads} at which U_{ads} is achieved (b) for systems II, III, IV.

order to find $\Omega(\mu)$ systems should be considered at two temperatures, one of which is supercritical. In the present work we have obtained the values of μ_{coex} at $T = 111$ K for different adsorbents and pore widths. Room temperature $T = 296.4$ K was chosen as a supercritical. Saturation pressures P_{coex} were derived from μ_{coex} taking into account second virial coefficients for methane (Reid et al., 1977).

3. Data Analysis

Molecular structure of the adsorbate can be characterized in different ways. First of all, we consider the overall density in the pore, defined as $\rho = \langle N \rangle / V$, where $\langle N \rangle$ is the average number of fluid molecules in the pore, $V = L_x L_y H$. Structure of the fluid in the direction normal to the walls z is described by the local

density profile $\rho(z)$:

$$\rho(z) = \frac{\langle N(z)\rangle}{A\triangle z}, \tag{3}$$

where $\langle N(z)\rangle$ is the average number of fluid molecules in a slice with the cross section A between z and $z + \triangle z$. We also consider the local energy profile $u(z)$, which is the average configurational energy per molecule in the slice. Density profiles for fluids in adsorbing pores are known to have distinct peaks corresponding to pronounced adsorbed layers. Each layer is characterized by its in-plane density $\Theta_i = \int_{z_{i-1}}^{z_i} \rho(z)\, dz$, where z_i and z_{i-1} are determined as neighboring minima of the local density, and the average configurational energy per molecule in the layer U_i. For each layer the in-plane pair correlation function $g_i(r)$ was calculated:

$$g_i(r) = \frac{\langle N_i(r)\rangle}{2\pi r \triangle r \Theta_i}, \tag{4}$$

where $\langle N_i(r)\rangle$ is the average number of fluid molecules at a distance between r and $r + \triangle r$ from a reference molecule in the same ith layer.

In order to see how the fluid molecules are distributed along heterogeneous coal surface for several systems we have calculated two-dimensional in-plane density profiles $\rho(x, y)$ for the nearest to the wall, contact, layer:

$$\rho(x, y) = \frac{1}{\Theta_1} \frac{\langle N_1(x, y)\rangle}{dx\, dy}, \tag{5}$$

where $\langle N_1(x; y)\rangle$ is the average number of fluid molecules in the contact layer with the coordinates $x \div x + dx$ and $y \div y + dy$.

Since the pores considered here are symmetrical, the figures show only a half of the pore space; z coordinates and the numbers of adsorbed layers are numerated from the walls.

4. Results and Discussion

4.1. Vapor-Liquid Coexistence

A subcritical isotherm is known to consist of several branches. Jumps between the branches correspond to layering, vapor-liquid and liquid-solid transitions in a pore. All these transitions were observed for system III; adsorption isotherms for system III at $T = 111$ K and various pore widths are shown in Fig. 3. One can see a fast increase of adsorption at $\mu = -13 \div -11\epsilon$ for $H = 6.0$, 8.0 and 10.0σ. This increase corresponds to a continuous formation of a single adsorbed layer on each wall. Within this interval adsorption isotherms for different pore widths almost coincide, as the interaction between opposite layers is negligible. This interaction becomes appreciable at $H = 4.0\sigma$: this pore is filled in one step without a monolayer formation. Similar dependence of the mechanism of pore filling on the pore width was observed for systems I (graphite) and II. No substantial influence of the adsorbent structure on the density of the adsorbed monolayer was found for systems I–III. It is necessary to mention that monolayer formation was also observed for 10-4-3 slit graphite pore (Jiang et al., 1993), but did not take place when 9-3 potential was used to present fluid-solid interactions (Piotrovskaya and Brodskaya, 1995). Simulations at $T = 0.5\epsilon/k$ (74.1 K) showed, that for systems II stable adsorbed monolayers can be obtained with the area of the basic cell of $42.65\sigma^2$ while for 10-4-3 potential a large cell (about $144\sigma^2$) is needed to obtain a stable adsorbed monolayer (Jiang et al., 1993, used the basic cell of $180\sigma^2$). Thus, surface defects in this case do not prevent monolayer formation, and can even stabilize an adsorbed monolayer.

Figure 4 shows the adsorption isotherms for system IV, which has more heterogeneous surface with weaker average adsorption field compared to system III. No formation of adsorbed monolayer takes place in this pore. Being filled with the increase of the chemical potential are the vacancies on the adsorbent surface, which are the preferential adsorbing sites. At the second stage capillary condensation occurs. However, a monolayer formation is observed for system V (Fig. 4(b)), which has smooth surface with the average parameters equal to those of system IV (Table 2). So, in this case surface heterogeneity destabilizes the adsorbed monolayer and even makes monolayer formation impossible.

The jump that follows the formation of monolayers, corresponds to the first-order vapor-liquid transition. On the basis the procedure mentioned in Section 2.4 chemical potentials of vapor-liquid phase coexistance μ_{coex} and condensation pressures P_{coex} for systems I–V have been calculated. They are shown in Table 3 along with the earlier results of Piotrovskaya and Brodskaya (1995) for uniform 9-3 pores (IP, IIP). For systems investigated at several H, the decrease of the saturation pressure on confinement was found, which is a characteristic tendency for slit wetted pores. The values of μ_{coex} for systems I, II and III are almost

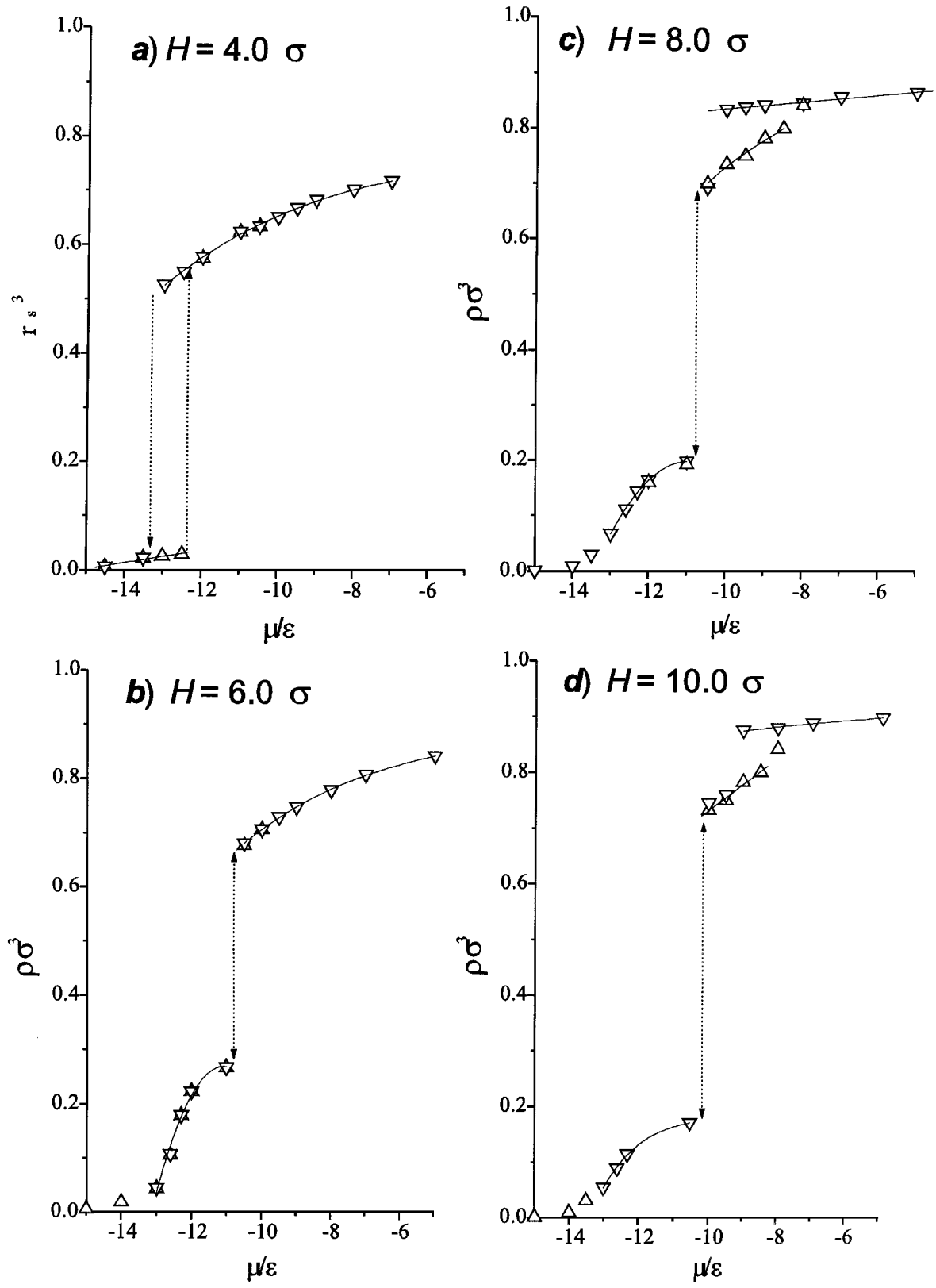

Figure 3. Adsorption (△) and desorption (▽) isotherms for system III for various pore widths at $T = 111$ K. (a) $H = 4.0\sigma$, (b) $H = 6.0\sigma$, (c) $H = 8.0\sigma$, and (d) $H = 10.0\sigma$.

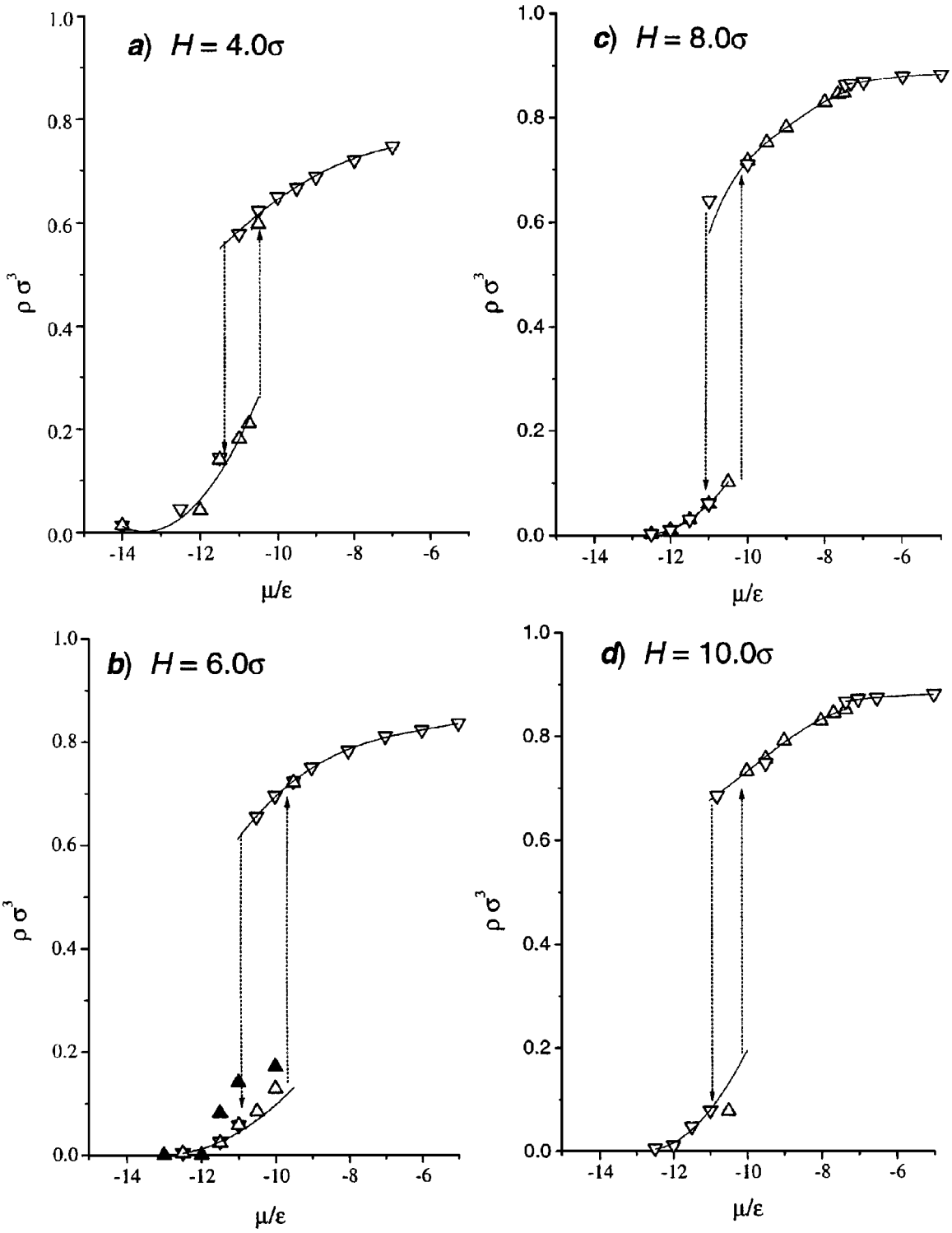

Figure 4. Adsorption (△) and desorption (▽) isotherms for system IV and various pore widths at $T = 111$ K. (a) $H = 4.0\sigma$, (b) $H = 6.0\sigma$, (c) $H = 8.0\sigma$, and (d) $H = 10.0\sigma$. Solid triangles in figure (b) show adsorption isotherm for system V.

Table 3. Chemical potentials of liquid-vapor phase coexistence μ_{coex} (ϵ) and saturation pressures P_{coex} related to the saturation pressure of bulk methane P^{∞} at T =111 K. Dashes denote that no capillary condensation is observed.

	$H = 4.0\sigma$		$H = 6.0\sigma$		$H = 8.0\sigma$		$H = 10.0\sigma$	
System	μ_{coex}/ϵ	P_{coex}/P^{∞}	μ_{coex}/ϵ	P_{coex}/P^{∞}	μ_{coex}/ϵ	P_{coex}/P^{∞}	μ_{coex}/ϵ	P_{coex}/P^{∞}
I	—		—		−10.62	0.23		
II	—		—		−10.57	0.24		
III	−12.1	0.031	−10.84	0.17	−10.64	0.22	−10.31	0.34
IP	—	—	−10.90	0.15	−10.65	0.22	−10.46	0.28
IV	−11.40	0.079	−10.31	0.34	−10.15	0.42	−9.84	0.64
V	—	—	−10.01	0.51	−9.95	0.55	−9.87	0.61
IIP	—	—	−9.95	0.55	−9.93	0.56	−9.88	0.60

equal, they lie within the statistical error. Apparently, the formation of adsorbed monolayers, preceeding the capillary condensation, diminishes the influence of the details of the surface microstructure on the conditions of the liquid-vapor equilibrium. It is only the contact adsorbed layer where the local density and local energy per molecule are affected by the surface inhomogeneity; for inner layers this influence is negligible (Fig. 5(a)). On the contrary to systems I–III, V, in system IV fluid molecules adsorb directly on the heterogeneous coal surface when the capillary condensation occurs; that is why the conditions of the coexistence get shifted related to system V. Local density and local energy profiles for systems IV and V are shown in Fig. 5(b). The minimum on the energy profile for system IV corresponds to the molecules adsorbed in "holes" on the surface (see Fig. 2); the location of such molecules is practically fixed. Filling of the holes by fluid molecules "strengthens" the adsorpton field. As a result of a nonuniform distribution of molecules along the surface, the energy per molecule in the system IV is lower than in system V. This effect is sensible even for the second adsorbed layer, though the fluid in the system IV is less structured in z direction. It results in lowering of the condensation pressure in the system IV relative to system V, with this lowering being pronounced only for quite narrow pores ($H = 6.0\sigma$). For $H = 10.0\sigma$ this effect is already insignificant.

Another result of a strong heterogeneity of the adsorbent surface in system IV is a significant hysteresis observed in this pore (Figs. 4(b)–(d)). For the systems I–III and V hysteresis loops are not evident (Figs. 3(b)–(d)). In these systems with the increase of the chemical potential, first adsorbed monolayers of the fluid cover the walls of the pore; during the capillary condensation fluid molecules interact mostly with these layers, which are practically plain in respect to energy. In system IV fluid condensates in a pore which is almost empty; the energies of separate molecules are quite different from each other. Significant energetical heterogeneity was found even in the second layer. Apparently, in such conditions condensation is controlled by the nucleation developing on the active adsorbing sites and vapor pressure above the convex meniscus is higher compared to that for the plane surface. This results in appearence of metastable states, producing a significant hysteresis loop.

4.2. Precondensation

In this section we consider capillary condensation in pores, where strongly adsorbing sites form symmetric strips on both walls of the pore. As it was shown by Gac et al. (1993), and Röcken and Tarazona (1996) the space between the strips is likely to be filled prior to the capillary condensation. This formation of a "neck" between adsorbing strips is called precondensation. It was shown that the ratio of the width of the adsorbing strip to the pore width plays a crucial role for the stability of the liqiud film over the strips. However, in the works mentioned above very simple models were used to present fluid-fluid and fluid-solid interactions: fluid was supposed to be a lattice gas with a square–well potential, and the strength of the adsorption field changed steeply inside the slit pore. Our aim is to determine the conditions, at which precondensation in slit carbon pores takes place, and to find whether the formation of the liquid "neck" is continuous or not. According to the objects chosen for the present work, we were restricted to our model of coal, pore widths $H = 6.0$–10.0σ at $T = 111$ K. The model of coal surface (system VI) is shown in Fig. 1(c).

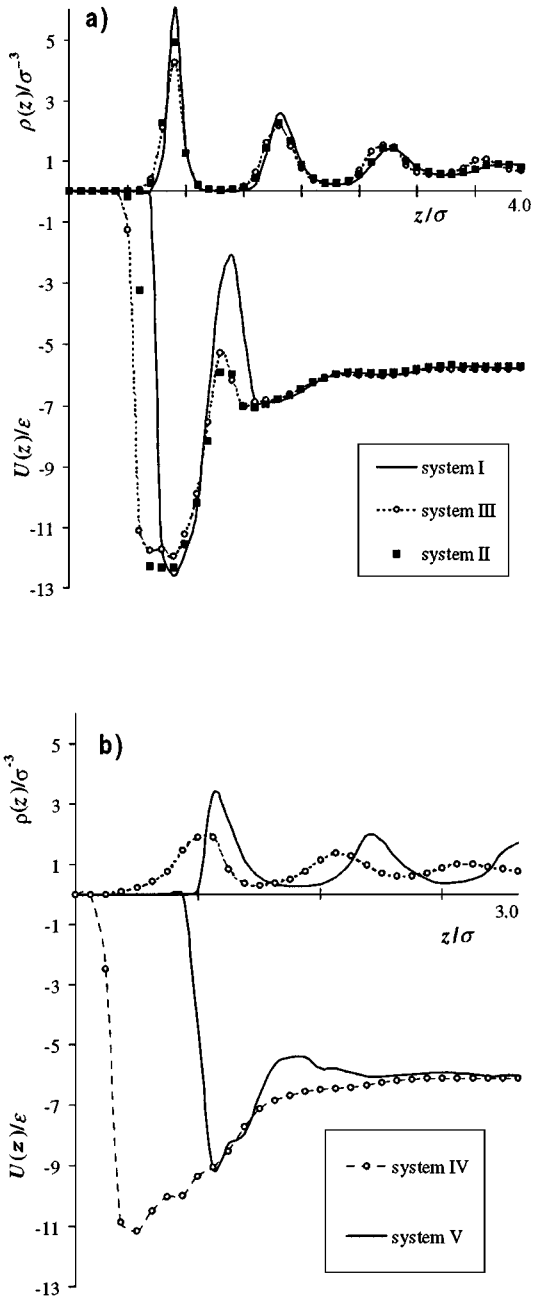

Figure 5. Local density and local energy per molecule at $T = 111$ K, $\mu = -10.0\epsilon$: (a) for systems I, II, III, $H = 8.0\sigma$; (b) for systems IV, V. $H = 6.0\sigma$

First of all, the ability of the pore to a monolayer formation was found to be crucial for precondensation. *No precondensation was observed in pores where adsorbed monolayers cover the walls over the weakly adsorbing part of the pore prior the capillary condensation.* Provided the distance between the adsorbing strips is large enough, this ability depends on U_{weak}, (see Section 2.2). The critical value of U_{weak} was found to be about -3.3ϵ. At lower values of U_{weak} adsorbed monolayers formed on the pore walls and capillary condensation occurred in one step.

Figure 6 shows the adsorption isotherms for the system VI, $U_{\text{weak}} = -3.3\epsilon$, $L_s = 4.8\sigma$ and different pore widths. Starting point $\mu = -14.0\epsilon$ corresponds to the state when a single monolayer has already formed over strongly adsorbing strips; the other part of the pore is almost empty. For $H = 6.0\sigma$ there was observed gradual filling of further adsorbed layers over the strongly adsorbing strips in the pore. Rise at $\mu = -11.5\epsilon$ corresponds to a continuous transition from one to two monolayers adsorbed over the strips (Fig. 6(a)). It should be noticed that for $H = 6.0\sigma$ the fluid in the "neck" consists of strongly pronounced adsorbed layers; the fluid structure in z direction becomes much less pronounced at $H = 7.2\sigma$. Nevertheless, precondensation still stays continuous. For $H = 8.3\sigma$ capillary condensation occurs in two jumps (Fig. 6(c)). The first corresponds to the first-order formation of a liquid "neck" between the strongly adsorbing strips, and the second one is the filling of the weakly adsorbing part of the pore. Snapshot of methane molecules after the first step is shown in Fig. 7. Finally, if we increase the pore width up to 9.6σ, one-jump capillary condensation is observed. No precondensation takes place in this case, though one can see the beginning of formation of the second adsorbed layer over the strongly adsorbing strips.

It should be noted that adsorption and desorption curves for the system VI do not coincide, indicating strong hysteresis effect. For example, for $H = 8.3\sigma$ fluid in the pore evaporates simultaneously in both parts of the pore with the decrease of the chemical potential from -10.8 to -10.6ϵ. Since the pore has a periodical structure, on the stage of precondensation the system is characterized by a large surface contribution to its free energy. This additional surface contribution makes adsorption and desorption isotherms to be different; as a result, evaporation of the fluid occurs in one stage for all pore withs considered.

For $L_s = 3.0\sigma$ a continuous formation of the "neck" was observed at $H = 6.0$ and 7.2σ, for $L_s = 2.4\sigma$—at $H = 6.0\sigma$ only. So, the pore width, at which precondensation can take place, decreases with the decrease of the widths of the adsorbing strip, in agreement with the conclusions of Röcken and Tarazona (1996). *No steep transitions were found for* $L_s = 2.4$ *and* 3.0σ. Such a dependence of the mechanism of the pore

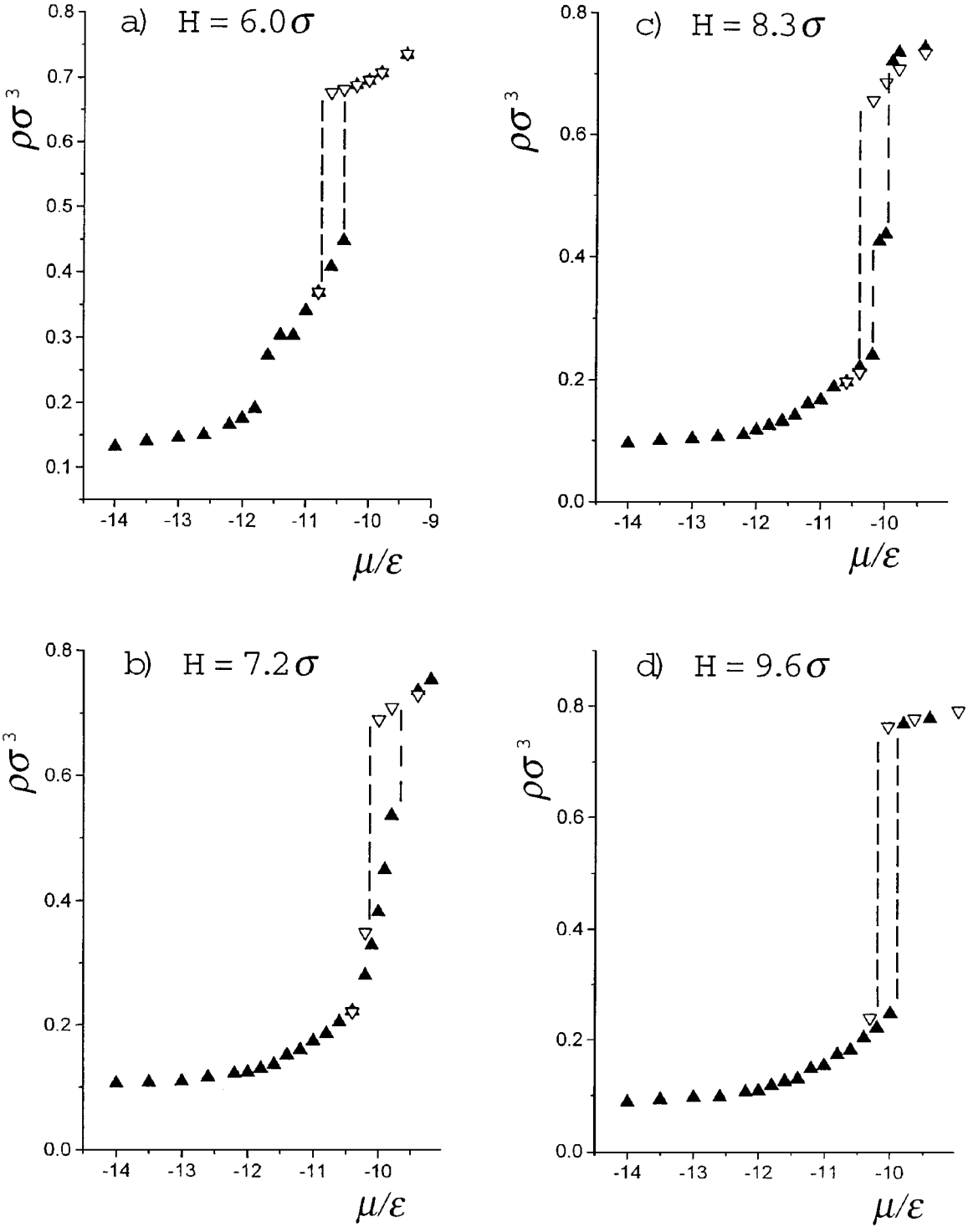

Figure 6. Adsorption (△) and desorption (▽) isotherms for system VI at $T = 111$ K. (a) $H = 6.0\sigma$, (b) $H = 7.2\sigma$, (c) $H = 8.0\sigma$, and (d) $H = 9.6\sigma$.

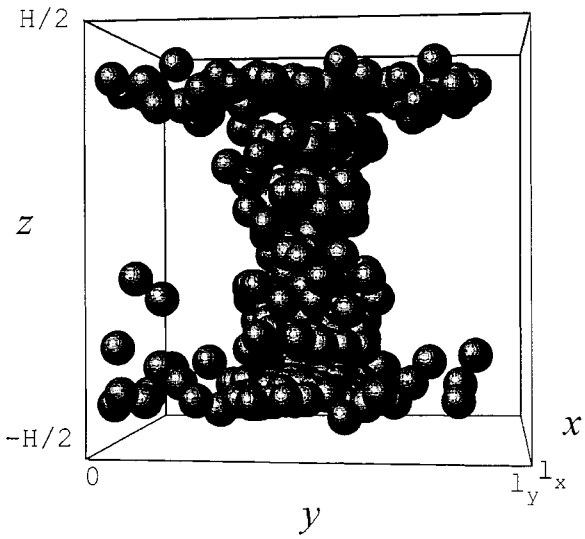

Figure 7. Snapshot of molecular positions for system VI, $H = 8.3\sigma$ at $\mu = -10.2\epsilon$ and $T = 111$ K. Methane forms a liquid-like "neck" between the strongly adsorbing strips.

filling on the strip width seems natural: obviously, at large L_s capillary condensation must occur in two jumps, corresponding to the condensation of a fluid in two parts separately.

4.3. Freezing and Melting

From Figs. 3 and 4 one can see that with the increase of the chemical potential after the capillary condensation, some discontinuities accompained by hysteresis loops, appear on adsorption isotherms. These discontionuities indicate liquid-solid transitions in pores.

The effect of the change in pressure on the freezing temperatures is known to be very weak for bulk fluids. So, it seems more appropriate to study melting and freezing by changing temperature. For fluids in pores an ideal method is heating and cooling of the system at a constant pressure of the bulk fluid, kept in equilibrium with the fluid in pore (P_{bulk}). However, P_{bulk} is difficult to fix in computer experiment with a nonuniform system, especially at temperatures below the bulk freezing point T_f^{∞}. That is why we have chosen the most straight way of changing the temperature at constant chemical potential, since the latter is fixed in the grand canonical ensemble. This method has two serious disadvantages. First, it does not correspond to any experimental procedure. Second, there is no simple way to determine the state of the bulk material at the same conditions. It should be also noted that the basic cell we use in this work ($6.405\sigma \times 6.660\sigma$) is not large enough for precise measurements of freezing and melting temperatures. Though we did not consider the dependence of the freezing temperature on the size of the basic cell, it, seems possible to make some qualitative conclusions concerning the influence of the surface inhomogeneity on the transition points comparing the results for corresponding pores with smooth and rough walls. Namely, we consider systems I and III, IV and V. Systems I and III have the adsorption field close to that of graphite pore, systems IV and V correspond approximately to "methane pore" of Miyahara and Gubbins (1997).

Several criteria were applied to locate freezing and melting points. First, steep changes in density and energy per molecule in a pore or in an individual adsorbed layer can be used as an indicator that a transition takes place. Then the type of the phase state of a fluid in pore can be confirmed on the basis of two-dimensional in-layer correlation functions $g(r)$ (see Section 3) and diffusion coefficients, since diffusion coefficients change by several orders in a layer which undergoes a melting or freezing transition. Snapshots of molecular configurations of individual layers can also be helpful. Note that the triple point for a Lennard-Jones fluid is $0.68\epsilon/k$ (Agraval and Kofke, 1995), which corresponds to 101 K for methane with the LJ parameters we use here. Experimental triple point for methane is 90.68 K (Sychev et al., 1979).

Figure 8 shows the variation of the overall density ρ on the temperature in system III at $\mu = -7.0\epsilon$. One can see abrupt changes in density at $H = 8.0\sigma$ and $H = 10.0\sigma$ both at heating and cooling curves. These changes correspond to methane melting and freezing in the pore and are accompained by corresponding changes in the energy per molecule. Cooling and heating curves do not coincide, forming pronounced hysteresis loops. True thermodynamic transition point cannot be determined on the basis of heating and cooling curves; however, the true transition is expected to lie within the hysteresis loop. Cooling curve is likely to give a better approximation to the true transition because of the greater success rate in molecule insertions and deletions on the cooling sequence (Miyahara and Gubbins, 1997). Variations of density in the pore on cooling and heating, shown in Fig. 8, are typical; similar variations were observed for systems I and V. All freezing temperatures obtained are shown in Table 4.

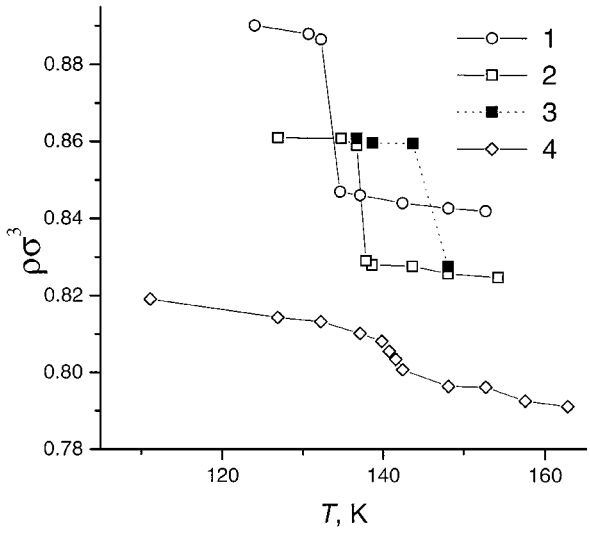

Figure 8. Dependence of the total density in the pore on temperature for system III at $\mu = -7.0\epsilon$. (1) $H = 10.0\sigma$, cooling; (2) $H = 8.0\sigma$, cooling; (3) $H = 8.0\sigma$, heating; (4) $H = 6.0\sigma$, cooling.

As it is seen from Table 4, freezing temperatures for corresponding pores with smooth and heterogeneous walls differ significantly from each other and show different dependence on the pore width. In system I the freezing temperature is higher related to that of the bulk material, and increases with the confinement. This result agrees with the conclusions of Miyahara and Gubbins (1997). At the same time in system III (typical anthracite) freezing temperatures are almost equal for different pore widths; at $\mu = -9.0\epsilon$ they are close to the triple point of the bulk fluid. Substantial differences

Table 4. Freezing temperatures for methane in pores (K).

	System			
H/σ	I	III	IV	V
		$\mu = -9.0\epsilon$		
6.0	$120.4 \pm 2.0^*$	$97.8 \pm 1.0^*$	92.8 ± 1.0	$101.8 \pm 3.0^*$
8.0	112.5 ± 2.0	99.8 ± 1.0	96.8 ± 1.0	100.8 ± 1.0
10.0	104.1 ± 2.0	99.8 ± 1.0	100.8 ± 1.0	102.8 ± 1.0
		$\mu = -7.0\epsilon$		
6.0	$154.0 \pm 2.5^*$	$139.5 \pm 2.5^*$		
8.0	145.5 ± 1.5	137.2 ± 0.5		
10.0	137.1 ± 1.5	133.4 ± 1.2		

*No clear transition was observed for these systems. Given in the table are approximate values, estimated from the dependence of the total density on temperature.

in the freezing temperature are also found between systems IV and V. Being similar to the "methane" pore of Miyahara and Gubbins (1997), system V does not show considerable changes in the freezing temperature with confinement. On the contrary, in system IV the freezing temperature is lower compared to that of the bulk material and decreases with the decrease of the width of the pore. In sequences I–III, V–IV a decrease in freezing temperature is observed at a given value of the pore width. Thus, irregular defects on the solid surface contribute to the decrease of the freezing temperature in slit pores and can even change qualitatively its dependence on the pore width.

In order to demonstrate the mechanism of the influence of the surface microstructure on the freezing temperature, let us consider the molecular structure of the adsorbate above and below the freezing point. As an example we have chosen system III at $H = 8.0\sigma$ and $\mu = -7.0\epsilon$ on the cooling sequence. Figure 9 shows local density and energy profiles at $T = 137.7$ K and $T = 136.7$ K; the freezing point lies somewhere in-between. It is seen that such a small decrease in temperature makes the fluid much more structured in the direction normal to the pore walls. At $T = 136.7$ K local density in all inner layers is almost equal, with the local density between the layers being close to zero (Fig 9(a)). With cooling from 137.7 to 136.7 K local energy per molecule in adsorbed layers decreases; location of a molecule between the layers becomes energetically unfavorable (Fig. 9(b)). Notice also, that only the density and the shape of the inner layers change significantly within this temperature interval, while the density and the shape of the contact layer remains almost the same (Figs. 9 and 10). Variation of the surface density and energy per molecule on cooling for individual layers show that the increase in the overall density observed with cooling from 137.7 to 136.7 K occurs in the inner layers (Fig. 10). In all inner layers local energy per molecule decreases steeply at cooling to 136.7 K, while no considerable changes in the first layer are observed. In-plane pair correlation functions for individual layers at 137.7 and 136.7 K show that at $T = 137.7$ K all inner layers have a liquid-like structure (Fig. 11(b)); at $T = 136.7$ K the structure in these layers becomes solid-like (Fig. 11(a)). As an example, snapshots of the fourth, innermost layer at both temperatures are shown in Fig. 12. At $T = 137.7$ K the layer shows a disodered state; at $T = 136.7$ K the molecules form a hexagonal array resembling the (111) face of a fcc lattice. At the same time in-plane pair correlation

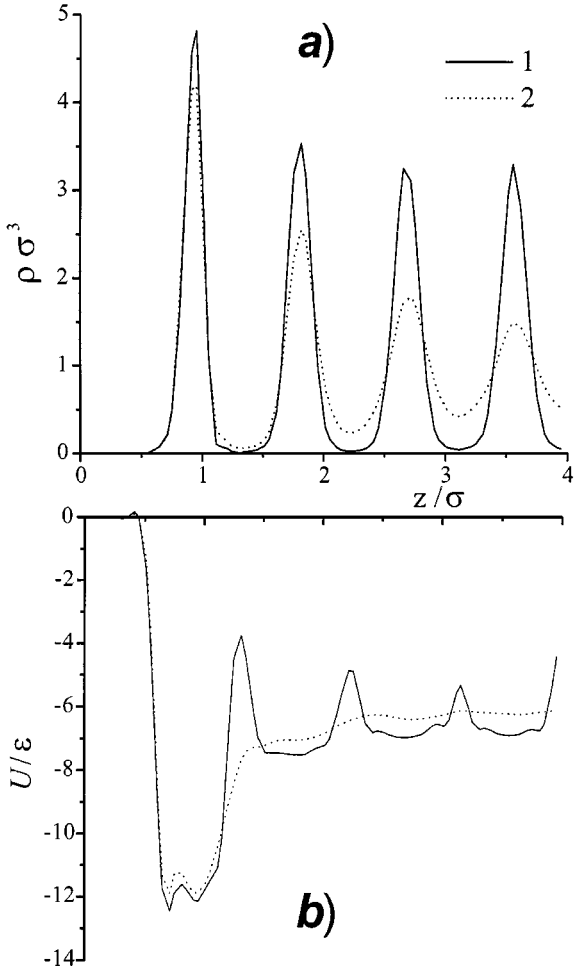

Figure 9. Local density (a) and local energy (b) profiles for system III, $H = 8.0\sigma$ at $\mu = -7.0\epsilon$ and $T = 136.7$ K (1) and $T = 137.7$ K (2).

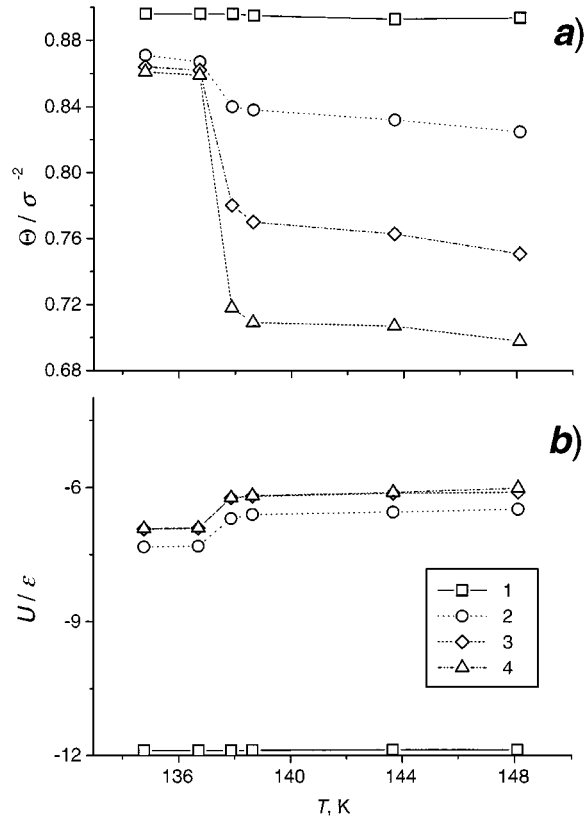

Figure 10. Dependences of the surface density Θ_i (a) and local energy per molecule (b) on temperature for individual adsorbed layers in system III. $H = 8.0\sigma$, $\mu = -7.0\epsilon$. (1) contact layer, (2) second layer, (3) third layer, (4) fourth, innermost layer.

functions for the contact layer are typical for the solid state at both temperatures (Fig. 11).

It is worth mentioning that no substantial difference in the freezing temperature between inner layers was found for systems I and III at $H = 8.0\sigma$ and $H = 10.0\sigma$. Some differences in freezing temperatures of the inner layers for graphite pores were observed by Miyahara and Gubbins (1997). However, it should be noted that freezing temperatures of individual layers were demonstrated at $H = 9.5\sigma$ and $H = 7.5\sigma$ (Miyahara and Gubbins, 1997). Both of these pores are characterized by relatively large average separation between the neighbouring adsorbed layers. Graphite pore at $H = 9.5\sigma$ contains nine adsorbed layers; the average separation between two adjacent layers is about 0.95σ. Systems I and III at $H = 10.0\sigma$ contain 10 layers each with the average separation of 0.90σ. Similar differences exist between the pores $H = 7.5\sigma$ and $H = 8.0\sigma$. Apparently, the larger the interlayer separation, the more independent is the behavior of the layers. In system III at $H = 8.0\sigma$ and $\mu = -7.0\epsilon$ the difference in the freezing temperatures of individual inner layers does not exceed 1 K.

We can see that the abrupt changes occurring in pore III for $H = 8.0\sigma$ do not affect the contact adsorbed layer. The density and the structuring of the contact layer at $H = 8.0\sigma$ and $\mu = -7.0\epsilon$ increase gradually with the cooling of the system from 145 to 125 K. No steep changes in density and structure of the contact layer were observed, though these steep changes are found to be characteristic for isolated adsorbed monolayers. The molecular structure of the contact layer can be described using in-plane density profile (5); for system III, $H = 8.0\sigma$, $\mu = -9.0\epsilon$ at $T = 111$ K it

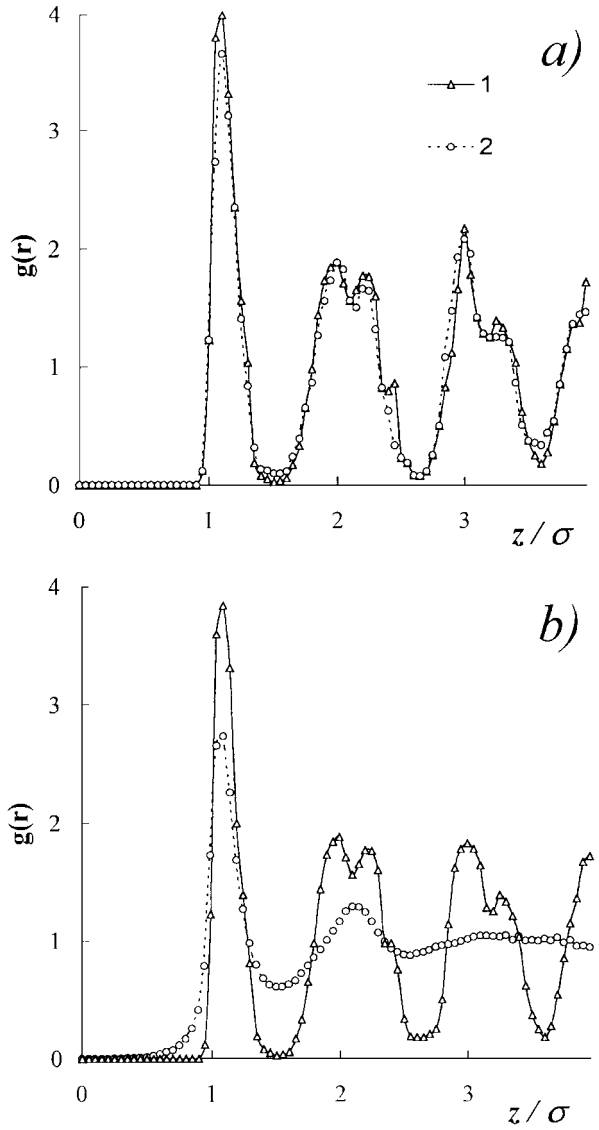

Figure 11. In-plane pair correlation function for the contact (1) and fourth (2) layers in system III, $H = 8.0\sigma$, $\mu = -7.0\epsilon$. (a) $T = 136.7$ K, (b) $T = 137.7$ K.

is shown in Fig. 13. It is seen that the layer has a pronounced hexagonal structure distorted considerably due to the defects on the coal surface. Mobility of the fluid molecules in this layer is limited. This prevents the structure of the first layer from being commensurate with that of the second layer, contributing to lowering in the freezing temperature of the fluid.

For $H = 6.0\sigma$ we failed to locate the freezing transition point in systems I and III, as well as in system V. Table 4 gives approximate values estimated from the dependence of the total density on temperature (see Fig. 8, curve 4). For example, in system III at $\mu = -7.0$ the density of the fluid in pore grows significantly with cooling of the system from $T = 142$ to 137 K (Fig. 8). The energy per molecule and structural characteristics change correspondingly, but no abrupt changes, indicating a first-order freezing transition were observed for entire pore or individual layers. At $H = 6.0\sigma$ in the system III methane forms five pronounced adsorbed layers with the average distance between the neighbouring layers about 1.25σ. Practically in this pore fluid consists of adsorbed layers only and does not have a three-dimensional liquid-like structure, observed for $H = 8.0\sigma$. This makes the behavior of inner layers more similar to the one of isolated adsorbed monolayers at rough surfaces. These effects seem to be similar to those for graphite pore at $H = 5.3\sigma$ of Miyahara and Gubbins (1997), but in the latter case they are much more pronounced.

Due to the strong surface heterogeneity in system IV, layered structure of the adsorbate is not pronounced. That is why freezing and melting transitions in this pore were fixed on the basis of abrupt changes in density, energy per molecule, and diffusion coefficient of the adsorbate with changes in temperature. For all values of the pore width considered evident melting and freezing transitions were observed in entire pore space, including the first adsorbed layer. For example, in the pore $H = 8.0\sigma$ at $\mu = -9.0\epsilon$ and $T = 101.8$ K we obtained $\rho = 0.835\sigma^{-3}$, average energy per molecule -7.11ϵ, and the diffusion coefficient in the direction parallel to the walls $D_{\|} = 2.3 \cdot 10^{-2}\sigma\sqrt{\epsilon/m}$, where m is the mass of methane molecule. After the decrease in temperature by 2 K the overal density increases up to $\rho = 0.863\sigma^{-3}$, the average energy per molecule decreases to -7.72ϵ, the estimation of the diffusion coefficient gives $D_{\|} < 10^{-6}\sigma\sqrt{\epsilon/m}$. Similar changes were found for $H = 6.0$ and 10.0σ. It should be noted that almost no hysteresis was obtained for system IV.

The freezing temperatures for methane in pores at different μ allow to estimate the influence of the pressure on the freezing point. The pressure of the bulk fluid in equilibrium with the fluid in a pore P_{bulk} can be derived from the temperature and chemical potential. If the state of the corresponding bulk fluid is a vapor or a liquid-like, the correlation between μ and P_{bulk} can be obtained using a simple analytical equation of state. Here we use Soave-Redlich-Kwong equation. Within the solid-state area of the phase diagram

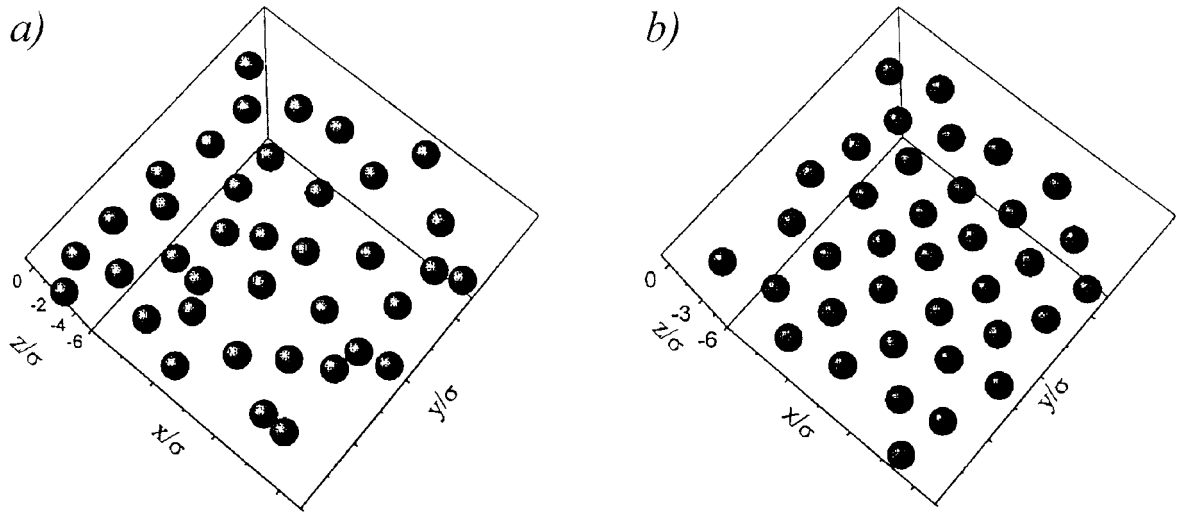

Figure 12. Snapshots of the molecular configurations of the fourth, innermost layer, in the system III, $H = 8.0\sigma$, $\mu = -7.0\epsilon$. (a) $T = 137.7$ K (disordered state), (b) $T = 136.7$ K (solid state).

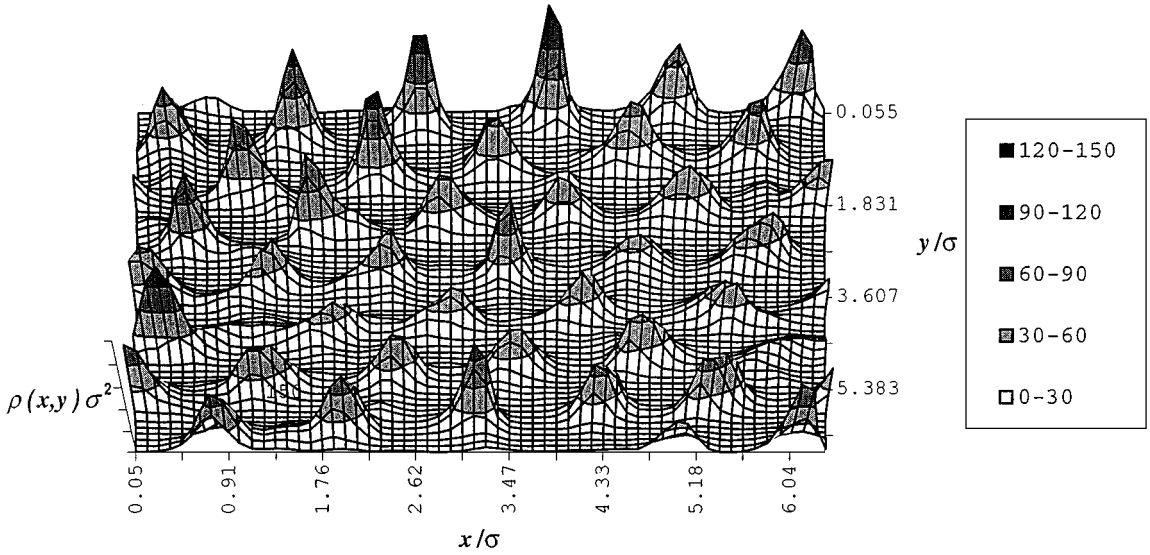

Figure 13. In-plane density profile for the contact layer in system III, $H = 8.0\sigma$, T =111 K, $\mu = -9.0\sigma$.

changes in pressure were estimated using the following expression:

$$dp = \rho \, d\mu \tag{6}$$

in assumption that the density of the solid methane is constant. For example at $T = 99.8$ K, which is the freezing point for methane in system III at $H = 8.0\sigma$ and $\mu = -9.0\epsilon$ we obtain $P_{\text{bulk}} = 0.99 \times 10^2$ Pa. For $\mu = -7.0\epsilon$ at $T = 137.2$ K $P_{\text{bulk}} = 1.11 \times 10^6$ Pa. Thus, with the increase of the pressure by 1 MPa the freezing temperature changes by 30 K. Estimation of the same value from the experimental data for methane (Sychev et al., 1979) gives the value of about 6 K, which is approximately five times lower. It makes us to suppose that the dependence of freezing points for the confined fluids is stronger relative to that for the bulk. It can be explained both by higher compressibility of fluids in pores and changes in the melting enthalpy on confinement.

5. Conclusions

Vapor-liquid and liquid-solid phase transitions for methane in slit pores with homogeneous and heterogeneous walls have been studied using GCMC technique. The pore wall heterogeneity can be of different kind and extent. Correspondingly, its influence on phase transitions in pores can also differ. In the present work we have considered slit pores, formed by mining coals of various metamorphism; the adsorbent surface was modeled as a basal graphite plane containing some impurities and vacancies (systems II–IV). We have also considered a structure with a periodic pore wall potential, where strongly adsorbing sites form a strip at the weakly adsorbing surface. Thus, the size of defects in systems II–IV is of the same order as the diameter of an adsorbate molecule; in system VI inhomogeneities have the size comparable to the pore width.

Simulations of capillary condensation in coal pores II–IV showed that the influence of the surface microstructure on the conditions of vapor-liquid phase coexistence depends strongly on the ability of the adsorbing surface to form an adsorbed monolayer. The saturation bulk pressure P_{coex} for systems II and III is practically equal to that for graphite pore (system I). Another picture was observed for system IV, where no monolayer formation takes place prior to capillary condensation. Equilibrium chemical potential μ_{coex} and saturation pressure for these pores are lower compared to those of the corresponding pores with smooth walls (V), especially for more narrow pores $H = 6.0\sigma$ and $H = 8.0\sigma$.

The mechanism of capillary condensation in system with a periodic wall potential VI was found to depend on the pore width and the adsorption fields of the strongly and weakly adsorbing parts of the pore. When the adsorption field of the weakly adsorbing part is strong enough to keep an adsorbed monolayer, one-step capillary condensation was observed for all pore widths considered. In the case when no monolayer formation took place in the weakly adsorbing part, two-stage capillary condensation was observed. The first stage corresponds to the formation of a narrow "neck" over the strongly adsorbing strips (precondensation), while the second one is the filling of the weakly adsorbing part of the pore. Dependent on the pore width and the width of the adsorbing strip, precondensation can be continuous or a first order.

To explore the influence of the surface inhomogeneity on freezing/melting phase transitions we have estimated the freezing temperatures of methane for systems I, III, IV, V. It was shown that irregular defects of the surface microstructure contribute to the lowering in freezing temperature and can even change qualitively its dependence on the pore width. For graphite pores (system I) the freezing temperature is higher than for the bulk methane, and increases with the confinement; this result agrees with the conclusions of Miyahara and Gubbins (1997). In the corresponding anthracite pore (system III) freezing temperatures are almost equal for different pore widths; at $\mu = -9.0\epsilon$ they are close to the triple point of the bulk fluid. Freezing temperatures in system IV were found to be lower than that of the bulk fluid and show increase with the increase of the pore width, while freezing temperatures in the corresponding pore with smooth walls V are practically equal to the bulk triple point for all pore widths considered. It is also shown that the influence of the pressure on the freezing temperature of a simple fluid in pores is more pronounced than that for the bulk fluid.

Nomenclature

A	Surface area	nm^2
g	In-plane pair correlation function	—
H	Pore width	nm
k	Boltzmann constant	J/K
$L_x,\ L_y$	Pore length in x and y directions	nm
L_s	Width of the strongly adsorbing strip	nm
N	Number of molecules	—
P	Pressure	J/m^3
$r_{\alpha\beta}$	Distance between two Lennard-Jones sites	nm
T	Temperature	K
ϵ	Energy parameter	J
Θ	Surface density	nm^{-2}
μ	Chemical potential	J/mol
ρ	Density	nm^{-3}
σ	Size parameter, diameter of core	nm

Subscripts

coex	Phase coexistence
f	Freezing
m	Melting
s	Solid
$\alpha,\ \beta$	Type of Lennard-Jones particle

Superscripts

∞ Equilibrium bulk system

Acknowledgment

This work has been partly supported by INTAS grant no. 1186. The authors are very thankful to Prof. W.A. Steele (Pennsylvania State University) for the useful disscussion of the work and for the possibility to carry out some of the calculations in his laboratory.

References

Agrawal, R. and D.A. Kofke, "Thermodynamic and Structural Properties of Model Systems at Solid-Fluid Coexistence. I. Fcc and bcc Lattice of Soft Spheres," *Mol. Phys.*, **85**, 43–51 (1995).

Bojan, M.J., R. van Slooten, and W.A. Steele, "Computer Simulation Study of Storage of Methane in Microporous Carbons," *Separ. Sci. and Tech.*, **27**, 1837–1843 (1992).

Eremin, I.V., V.V. Lebedev, and D.A. Tzikarev, *Petrograficheskie i Fizicheskie Svoistva Ugley*, Nedra, Moscow, 1980.

Proceedings of the Fourth International Conference on Fundamentals of Adsorption, M. Suzuki (Ed.), Engineering Foundation, New York, 1993.

Gac, W., A. Patrikeev, and S. Sokolovsky, "Influence of Surface Heterogeneity on Capillary Condensation in Slit Pores: A Monte Carlo Study," *Surface Sci.*, **306**, 434–446 (1994).

Jiang, Sh., C.L. Rhykerd, and K.E. Gubbins, "Layering, Freezing, Capillary Condensation and Diffusion of Methane in Slit Carbon Pores," *Mol. Phys.*, **79**, 373–391 (1993).

Jorgensen, W.L., "Potential Functions for Liquid Alchohols," *J. Phys. Chem.*, **90**, 1276–1288 (1986).

Jorgensen, W.L. and J. Gao, "Monte Carlo Computer Simulation of Hidration of Ammonium and Carboxilate Ions," *J. Phys. Chem.*, **90**, 2174–2182 (1986).

Jorgensen, W.L., J.D. Madura, and C.J. Swenson, "Optimized Intermolecular Potential Functions for Liquid Hydrocarbons," *J. Amer. Chem. Soc.*, **106**, 6638–6646 (1984).

Klein, J. and E. Kumacheva, "Confinement-induced Phase Transitions in Simple Liquids," *Science*, **269**, 816–819 (1995).

Miyahara, M. and K.E. Gubbins, "Freezing/Melting Phenomena for Lennard-Jones Methane in Slit Pores," *J. Chem. Phys.*, **106**, 2865–2880 (1997).

Molz, E., A.P.Y. Wong, M.H.W. Chan, and R.J. Beamish, "Freezing and Melting of Fluids in Porous Glasses," *Phys. Rev. B.*, **48**, 5741–5756 (1993).

Morishige, K., M. Fujii, M. Uga, and D. Kinukama, "Capillary Critical Point of Argon, Nitrogen, Oxygen, Ethilene, Carbon Dioxide in MCM-41," *Langmuir*, **13**, 3494–3498 (1997).

Müller, E.A., L.F. Rull, L.F. Vega, and K.E. Gubbins, "Adsorption of Water on Activated Carbon: A Molecular Simulation Study," *J. Chem. Phys.*, **100**, 1189–1198 (1996).

Peterson, B.K. and K.E. Gubbins, "Phase Transitions in a Cylindrical Pore. Grand Canonical Monte Carlo, Mean Field Theory and the Kelvin Equation," *Mol. Phys.*, **62**, 215–226 (1987).

Peterson, B.P., G.S. Heffelfinger, K.E. Gubbins, and F. van Swol, "Layering Transitions in Cylindrical Pores," *J. Chem. Phys.*, **93**, 679–685 (1990).

Piotrovskaya, E.M. and E.N. Brodskaya, "Computer Simulation of Two-Phase Equilibrium of Methane in Narrow Slit Wetted Pores," *Langmuir*, **11**, 642–645 (1995).

Reid, R.C., J.M. Prausnitz, and T.K. Sherwood, *The Properties of Gases and Liquids*, McGraw-Hill Book Company, New York, 1977.

Röcken, P. and P. Tarazona, "Capillary Condensation in Structured Pores," *J. Chem. Phys.*, **105**, 2034–2043 (1996).

Steele, W.A., *The Interaction of Gases with Solid Surfaces*, Pergamon, Oxford, 1974.

Steele, W.A. and M.J. Bojan, "Computer Simulation Study of Sorption in Model Cylindrical Pores," *Fundam. of Adsorption*, M.D. LeVan (Ed.), pp. 17–32, Kluwer Academ. Publ., Boston, 1996.

Sychev, V.V., A.A. Vasserman, and V.A. Zagoruchenko, *Thermodynamic Properties of Methane*, Izd. Standartov, Moscow, 1979.

Thommes, M. and G. Findenegg, "Pore Condensation and Critical Point Shift of a Fluid in Controlled-Pore Glass," *Langmuir*, **10**, 4270–4278 (1994).

Unruh, K.M., T.E. Huber, and C.A. Huber, "Melting and Freezing Behaviour of Indium Metal in Porous Glass," *Phys. Rev. B*, **48**, 9021–9031 (1993).

Warnock, J., D. Awschalom, and M.W. Shafer, "Geometrical Supercooling of Liquid in Porous Glass," *Phys. Rev. Lett.*, **57**, 1753–1759 (1986).

Weiner, S.J., P.A. Kolleman, D.A. Case, C.U. Singh, C. Ghio, G. Alagona, S. Profeta, Jr., and P. Weiner, "A New Force Field for Molecular Mechanical Simulation of Nucleic Acids and Proteins," *J. Am. Chem.* Soc., **106**, 765–784 (1984).